On the control of desiccant wheels in low temperature drying processes

Stefano De Antonellis *, Manuel Intini, Cesare Maria Joppolo, Francesco Romano
Dipartimento di Energia, Politecnico di Milano, Via Lambruschini, 4, 20156 Milan, Italy

Desiccant wheel based air handling units are of great interest in drying processes, such as in the pharmaceutical and food industries, due to the significant energy savings that can be achieved compared to conventional systems. Units based on desiccant wheels are usually optimized in peak conditions, while little attention is given to operation at part load and off design conditions. The aim of this work is to analyze the effects of different control strat-egies of desiccant wheels on regeneration heat consumption. The analysis is performed through a phenomenological desiccant wheel model, which is validated with experimen-tal data collected in typical working conditions of the drying room investigated in this work. Five control strategies are proposed, highlighting that each one leads to significantly dif-ferent heat consumption. Finally, an additional simplified control is introduced, showing that it can effectively reduce thermal power consumption compared to conventional control strategies.

Keywords: Desiccant wheel, Drying Simulation, Control, Off-design, Part load

Régulation des roues déshydratantes dans le processus de séchage à basse température

Mots clés : Roue déshydratante ; Séchage ; Simulation ; Régulation ; Hors-conception ; Charge partielle

1. Introduction

Desiccant evaporative cooling (DEC) cycles are of great interest due to the possibility of realizing low environmental impact HVAC systems, which can be driven by low temperature heat and renewable sources (Ge et al., 2014; Daou et al., 2006). Such technology is particularly suitable for air cooling and dehumidification processes, due to the possibility of exploiting low grade heat (Jeong et al., 2011; White et al., 2011) and of realizing high energy efficiency systems (Bourdoukan et al., 2010; Elgendy et al., 2015; Goldsworthy and White, 2011; Ling et al., 2013; Liu et al., 2007). In these systems, air dehumidification is generally obtained through a desiccant wheel, which is a rotating honeycomb device made of a supporting material coated with an adsorbent substance. The device is crossed in counter current arrangement by two air streams: the process air, which is dehumidified and heated, and the regeneration air, which removes water from the honeycomb structure.

Article history:
Received 30 March 2016
Received in revised form 20 June 2016
Accepted 22 June 2016
Available online 23 June 2016

* *Corresponding author.* Dipartimento di Energia, Politecnico di Milano, Via Lambruschini, 4, 20156 Milan, Italy. Fax: +39 02 23993913.
E-mail address: stefano.deantonellis@polimi.it (S. De Antonellis).

Nomenclature

Acronyms

COP	coefficient of performance [–]
MRC	specific moisture removal capacity [kg s^{-1} m^{-2}]
GSR	gas side resistance
DEC	desiccant evaporative cooling

Symbols

$A_{DW,tot}$	desiccant wheel total cross section area [m^2]
A	net channel area [m^2]
cp	specific heat [J kg^{-1} K^{-1}]
EXP	experimental
D	mass diffusivity [m^2 s^{-1}]
D_h	net channel hydraulic diameter [m]
f	mass per unit of length [kg m^{-1}]
h	enthalpy [J kg^{-1}]
h_T	heat transfer coefficient [W m^{-2} K^{-1}]
h_m	mass transfer coefficient [kg m^{-2} s^{-1}]
k	thermal conductivity [W m^{-1} K^{-1}]
L	desiccant wheel length [m]
$\dot{m}$	mass flow rate [kg s^{-1}]
N	revolution speed [rev h^{-1}]
Nu	Nusselt number [–]
NUM	numeric
P	inner channel perimeter [m]
q_{reg}	specific power for regeneration [W m^{-2}]
Q_{ads}	isosteric heat of adsorption [J kg^{-1}]
Sh	Sherwood number [–]
t	time [s]
T	temperature [°C]
v	face air velocity [m s^{-1}]
v'	channel air velocity [m s^{-1}]
W	water content [kg kg^{-1}]
X	humidity ratio [kg kg^{-1}]
z	channel length [m]

Greek symbols

ΔT_{pro}	process flow temperature rise [°C]
ΔX_{pro}	process flow humidity ratio drop [kg kg^{-1}]
λ	latent heat of vaporization [J kg^{-1}]
ρ	density [kg m^{-3}]
σ	wheel porosity [–]
φ	relative humidity [–]

Subscripts

a	ambient (drying room) air
ads	adsorbed water
D	desiccant
e	outdoor air
FD	fully developed flow
in	inlet
max	maximum at design conditions
min	minimum
out	outlet
opt	optimal
pro	process air
reg	regeneration air
w	channel wall

Drying processes require a proper control of air humidity and temperature in order to obtain the desired product quality. The use of desiccant wheels has been widely investigated for product drying (Dai et al., 2002; Misha et al., 2015; Nagaya et al., 2006; Wang et al., 2011) and it has been highlighted that significant energy savings can be achieved (De Antonellis et al., 2012). However, little attention is focused on how optimal control of desiccant wheels can be performed. Over the entire operating life, desiccant units mainly work far from design conditions: in fact they typically work at off-design and part load conditions, due to the variation of outdoor air and latent load conditions. It is well known that desiccant wheel performance is strongly affected by operating parameters, namely air flow rates, regeneration temperature and revolution speed, as shown in many research works (Chung et al., 2009; De Antonellis et al., 2010; Lee and Kim, 2014; Ruivo et al., 2007). Therefore, system efficiency can significantly decrease if desiccant wheel operating parameters are not controlled properly.

At present, recent research works on desiccant wheel mainly focus on phenomenological models, simplified correlations, experimental tests, new materials, innovative system configurations and potential energy savings, as clearly summarized in recent review papers (Rambhad et al., 2016; Sultan et al., 2015; Zouaoui et al., 2016). Instead, little attention is addressed to the optimization of operating parameters in off design and part load working conditions. A few works deal with the analysis and discussion of the control strategy and related performance of desiccant systems. New control strategies have been proposed for desiccant wheels-based systems for air conditioning purpose (Panaras et al., 2011; Vitte et al., 2008) or have been discussed in case of energy efficiency analysis of complex trigenerative systems (Angrisani et al., 2011; Hands et al., 2016; Intini et al., 2015). Anyway, in these works, the analyses focus on the entire system control, while the desiccant wheel dehumidification capacity is typically controlled as in conventional applications, modulating the regeneration air temperature at constant regeneration air flow or vice versa.

Due to the substantial lack of work in this field, in this paper, different desiccant wheel control strategies are evaluated in a low temperature product drying application. The analysis is performed considering five different control strategies that act on the following operating parameters:

- Regeneration temperature.
- Regeneration air flow rate.
- Wheel revolution speed.

Performance of each proposed control strategy is compared and, finally, an additional simplified control method is proposed.

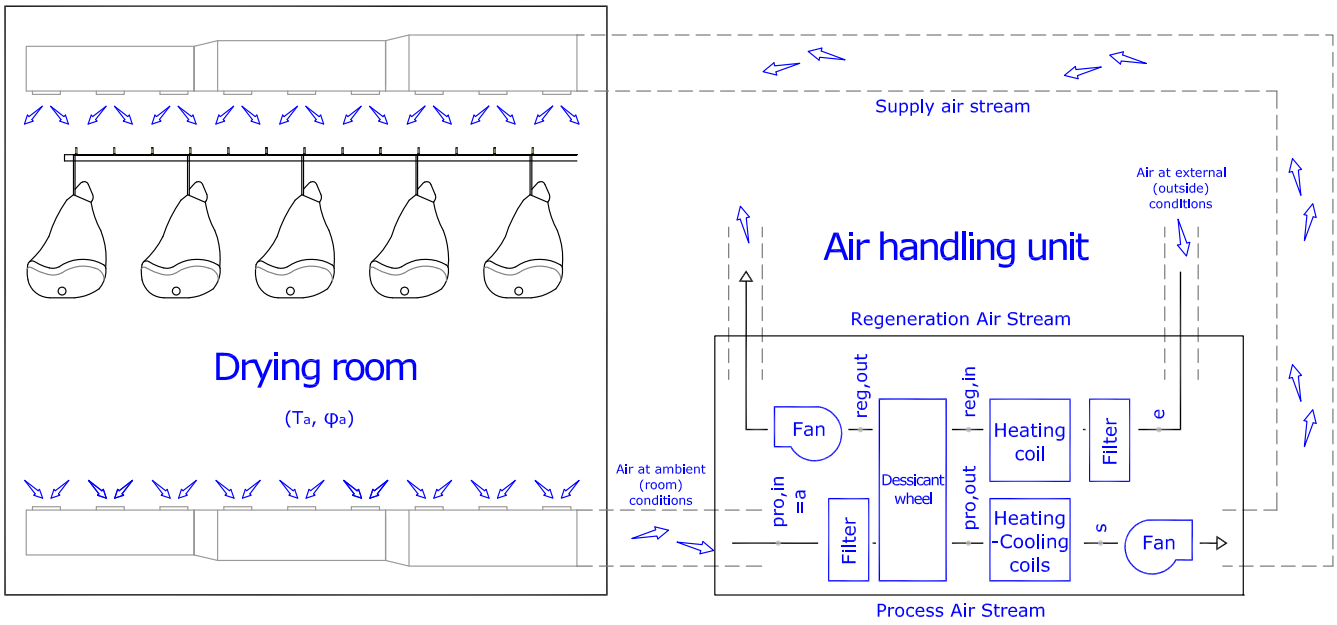

Fig. 1 – Scheme of the investigated desiccant cooling system for drying processes.

2. Description of the investigated system

As shown in Fig. 1, a room for food drying processes is chosen as reference case study (De Antonellis et al., 2012). The room is assumed at constant ambient conditions, more precisely at $T_a = 18$ °C and $X_a = 9.9$ g kg^{-1}, and the desiccant wheel based air handling unit works in recirculating mode. The process air stream is extracted from the drying room (condition *a*) and dehumidified across the desiccant wheel (from condition *a* = *pro,in* to condition *pro,out*). Then process air temperature is adjusted through a heating/cooling coil and it is supplied back to the drying room (from condition *pro,out* to condition *s*). The regeneration air stream is first heated through a heating coil (from outdoor condition *e* to condition *reg,in*), then it is cooled and humidified across the desiccant wheel (from *reg,in* to *reg,out*).

The process air flow face velocity is assumed equal to 2 m s^{-1}, which is a common value for desiccant cooling applications (De Antonellis et al., 2015a), while the regeneration one, depending on the investigated control system, is set equal or lower than 2 m s^{-1}. Desiccant cooling units for drying processes are mostly coupled with standard boilers or combined heat and power units. The regeneration air stream is heated in water heat exchangers, whose supply temperature typically ranges between 70 °C and 90 °C, depending on the heat source. For this reasons, in the present case study the maximum regeneration air temperature has been assumed to be 60 °C (inlet water temperature equal to 70 °C). Owing to the low regeneration temperature, the desiccant wheel area is equally split between process and regeneration air flows (Intini et al., 2014).

3. Methodology

The analysis reported in this research work has been performed through the following approach:

- A desiccant wheel has been tested in the laboratory facility. Measurements have been carried out in representative working conditions of the investigated drying room, which are different from the ones of conventional DEC cycles for air conditioning purposes.
- It has been verified that numerical results of the phenomenological desiccant wheel model, previously developed (De Antonellis et al., 2010) and calibrated (De Antonellis et al., 2015b), were in agreement with the experimental data collected in this work.
- Five different control strategies have been defined. It has been assumed that each control can act on one or more of the following parameters: regeneration temperature, regeneration air flow rate and revolution speed.
- Simulations are performed to evaluate the optimal system configuration while the effect of outdoor temperature, humidity and latent load are independently evaluated. The control strategies are compared in terms of coefficient of performance at constant moisture removal capacity.
- Finally, a simplified control approach is proposed and it is compared to the other five strategies for different latent loads and outdoor conditions.

3.1. *Test facility and adopted desiccant wheel*

The experimental setup consists of two air handling units that have been designed to control temperature, humidity and mass flow rate of process and regeneration air streams. The test rig has been deeply described in previous works of the authors (De Antonellis et al., 2015a, 2015b). Air temperature and humidity are controlled through heating coils, cooling coils, evaporative coolers and an electrical heater, while air flow rates are controlled by variable speed fans. Each air flow rate is measured through two orifice plates installed in two different parallel ducts and constructed according to technical standards (DIN EN ISO 5167-2 Standards, 2003). The maximum

Table 1 – Sensors main data.

Quantity	Type of sensor	Accuracy[a]
Temperature[b]	PT 100 Class A	±0.2 °C
Relative humidity[b]	Capacitive	±1% (between 0 and 90%)
Differential pressure	Piezoresistive	±0.5% of reading ±1 Pa

[a] At T = 20 °C.
[b] Temperature and relative humidity probe.

process air flow rate is 2000 $m^3\ h^{-1}$ and the maximum regeneration air flow rate is 1400 $m^3\ h^{-1}$. The desiccant wheel is crossed in counter-current arrangement by the two air streams and its casing is made of chipboards insulated with polystyrene panels (30 mm thickness).

Temperature and relative humidity of each air stream are measured at the inlet and at the outlet section of the casing with coupled RTD PT100 and humidity capacitive sensors. Pressure drop across the orifices installed in ducts is measured by piezoresistive transmitters (Table 1).

The tested desiccant wheel is a commercial device made of synthesized metal silicate on inorganic fiber substrate. Its outer diameter and length are respectively equal to 0.6 m and 0.2 m. The component is split in two equal sections without any purge sector. Channels have a sinusoidal cross sectional area (gross height equal to 1.8 mm and gross base equal to 3.55 mm).

Tests are performed in steady state conditions, collecting in each session at least 300 samples of every physical quantity with a frequency of 1 Hz. The experimental uncertainty of each measured and calculated quantity is estimated according to the international standards (ISO IEC Guide 98-3, 2008). The accuracy of temperature, relative humidity and pressure sensors is reported in Table 1.

3.2. *Model description and validation*

Simulations have been carried out through a one-dimensional gas side resistance (GSR) model. Main model assumptions are:

- One-dimensional air flow.
- Uniform air temperature, humidity and velocity at inlet faces of the wheel.
- Negligible heat and mass transfer between adjacent channels and to the surroundings.
- Negligible axial heat conduction and water vapor diffusion in the air stream and in the desiccant material.
- Negligible air leakages and carryover between the air streams.

The following equations have been applied to an infinitesimal element of the desiccant wheel channel.

Energy and water mass conservation in the desiccant material and in the adsorbed water:

$$(f_D\ cp_D + f_D cp_{ads} W_D)\frac{\partial T_D}{\partial t} = (cp_v(T_a - T_D) + Q_{ads})h_m(X - X_w)P + h_T(T_a - T_D)P \quad (1)$$

$$\frac{\partial W_D}{\partial t} = \frac{h_m(X - X_w)P}{f_D} \quad (2)$$

Table 2 – Main desiccant wheel data.

Parameter	Value	
P	7.8	[mm]
A	2.42	[mm^2]
Nu_{FD}	2.1	[–]
Sh_{FD}	2.1	[–]
$\sigma\ (v_{in}/v')$	0.76	[–]
cp_D	2.64	[kJ $kg^{-1}\ K^{-1}$]
f_D	0.00040	[kg m^{-1}]
L	0.2	[m]

Energy, water mass and dry air mass conservation in the air stream:

$$\frac{\partial T_a}{\partial t} = -v'\frac{\partial T_a}{\partial z} - \frac{h_T(T_a - T_D)P}{cp_a\ \rho_a\ A} - \frac{h_m(X - X_W)P cp_v T_a}{cp_a\ \rho_a\ A} \quad (3)$$

$$\frac{\partial X}{\partial t} = -\frac{\partial X}{\partial z}v' - \frac{P\ h_m}{\rho_a A}(X - X_w) \quad (4)$$

$$\frac{\partial \rho_a}{\partial t} = -\frac{\partial(\rho_a v')}{\partial z} \quad (5)$$

The isosteric heat of adsorption Q_{ads} has been assumed equal to the latent heat of vaporization of water and the specific heat of adsorbed water cp_{ads} has been considered equal to the one of liquid water. The heat and mass transfer coefficients are calculate respectively as $h_T = Nu\ k/D_h$ and $h_m = Sh\ \rho_a\ D/D_h$. The local Nusselt number Nu is calculated as a function of the Nusselt number at fully developed flow conditions Nu_{FD} and of the Graetz number, as proposed in literature (De Antonellis et al., 2010). Finally, the Lewis number is assumed constant and equal to 1 and, therefore, the local Sherwood number Sh is equal to the local Nusselt number Nu. All the adopted values are summarized in Table 2.

The adsorption isotherm of a sample of the desiccant wheel (metal silicate on inorganic fiber substrate) is represented in this form (De Antonellis et al., 2015b):

$$\varphi = 2.28\ W_D^{0.97} + 213.4\ W_D^{5.67} \quad (6)$$

A detailed description of adopted assumptions, governing equations (Eqs. 1–5), boundary and initial conditions and closure equations are reported in previous works of the authors (De Antonellis et al., 2010, 2015b).

Several experimental tests have been performed in typical working conditions of the investigated drying process. Process air inlet conditions are set equal to the adopted ambient conditions of the drying room, that are $T_{pro,in} = T_a = 18$ °C and $X_{pro,in} = X_a = 9.9$ g kg^{-1}. Face velocity of both air flows is $v_{pro,in} = v_{reg,in} = 2$ m s^{-1} and regeneration air humidity ratio is $X_e = X_{reg,in} = 15$ g kg^{-1}, corresponding to outdoor air at $T_e = 32$ °C and $\varphi_e = 50\%$. Model results show good agreement with data collected at variable revolution speed as well as with variable regeneration temperature. In Fig. 2 the quantities $\Delta X_{pro} = X_{pro,in} - X_{pro,out}$ and $\Delta T_{pro} = T_{pro,out} - T_{pro,in}$ are reported: the maximum deviation between the calculated (SIM) and measured (EXP) values are respectively equal to 0.3 g kg^{-1} and 1.2 °C.

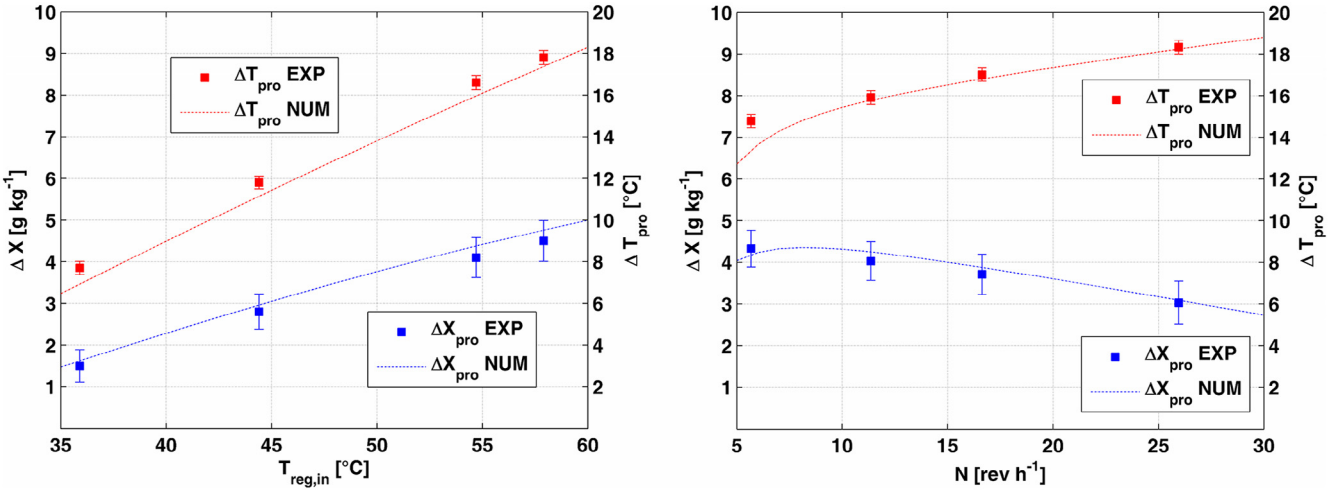

Fig. 2 – Comparison between model results and experimental data as a function of regeneration temperature (left, N = 11.4 rev h^{-1}) and revolution speed (right, $T_{reg,in}$ = 55 °C). Desiccant wheel main data are summarized in Table 2.

3.3. *Performance indexes*

Three different performance indexes are adopted in the present analysis, namely the moisture removal capacity MRC, the specific thermal power for regeneration and the coefficient of performance COP, defined in the following way:

$$MRC = \frac{\dot{m}_{pro}\left(X_{pro,in} - X_{pro,out}\right)}{A_{DW,tot}} = \frac{v_{pro,in}\rho_{pro,in}\left(X_{pro,in} - X_{pro,out}\right)}{2} \quad (7)$$

$$q_{reg} = \frac{\dot{m}_{reg}cp_{reg}\left(T_{reg,in} - T_e\right)}{A_{DW,tot}} = \frac{v_{reg,in}\rho_{reg,in}cp_{reg}\left(T_{reg,in} - T_e\right)}{2} \quad (8)$$

$$COP = \frac{\dot{m}_{pro}\left(X_{pro,in} - X_{pro,out}\right)\lambda}{\dot{m}_{reg}cp_{reg}\left(T_{reg,in} - T_e\right)} = \frac{v_{pro,in}\rho_{pro,in}\left(X_{pro,in} - X_{pro,out}\right)}{v_{reg,in}\rho_{reg,in}cp_{reg}\left(T_{reg,in} - T_e\right)} \quad (9)$$

where $A_{DW,tot}$ is the total face area of the desiccant wheel (equally divided between process and regeneration air flows). The MRC conveys the specific dehumidification capacity of the desiccant wheel, since it is proportional to latent heat removed from the process flow. Instead, q_{reg} is the regeneration power per unit of desiccant wheel area and COP is a direct indication of the efficiency of the process.

In this work, the proposed control strategies are compared in terms of COP, at given boundary conditions and MRC. It is highlighted that the electric power consumption related to ventilation and wheel rotation differs only slightly between the different control approaches and depends on the specific application (for example due to air filtration issues and consequent air pressure drop). Similarly, in Eqs. (8) and (9) only the thermal power required to regenerate the desiccant wheel is considered. Of course further heating or cooling of the supply air stream, which depends on the specific application and equipment setup, is required to balance the sensible load of the drying room, leading to an increase in the total power consumption. Therefore, in order to keep results as general as possible, such contributions have not been included in the analysis.

4. Results and discussion

4.1. *Reference conditions and preliminary analysis about system design*

According to the information provided in section 3, the desiccant wheel based system is designed considering the following boundary conditions and constraints:

- The drying room is assumed at the following conditions (typical raw ham and salami drying condition): T_a = 18 °C and X_a = 9.9 g kg^{-1} (φ_a = 77%, generally in the range between 75% and 80%).
- Inlet process air conditions are equal to drying room ambient conditions: $T_{pro,in} = T_a$ = 18 °C and $X_{pro,in} = X_a$ = 9.9 g kg^{-1}.
- Outdoor air is assumed at T_e = 32 °C and φ_e = 50% (X_e = 15 g kg^{-1}), which is typical summer peak condition in cities located in Northern Italy, such as Milan.
- Inlet regeneration air humidity ratio is equal to outdoor air humidity ratio ($X_{reg,in} = X_e$ = 15 g kg^{-1}).
- It is assumed that the inlet regeneration air temperature can be varied and raised up to maximum 60 °C.
- The process air face velocity is assumed equal to 2 m s^{-1}, which is a typical value of real applications.
- The desiccant wheel revolution speed can be adjusted between 5 rev h^{-1} and 26 rev h^{-1}, according to limits of the device tested in section 3.2.

Considering the aforementioned boundary conditions and constraints, the desiccant wheel performance depends on the regeneration air temperature, regeneration air velocity and revolution speed. The design of the desiccant wheel can be performed in different ways, maximizing MRC, COP or in an intermediate configuration. Once operating conditions are selected, an appropriate wheel size (diameter) should be determined in order to match the latent load of the drying room.

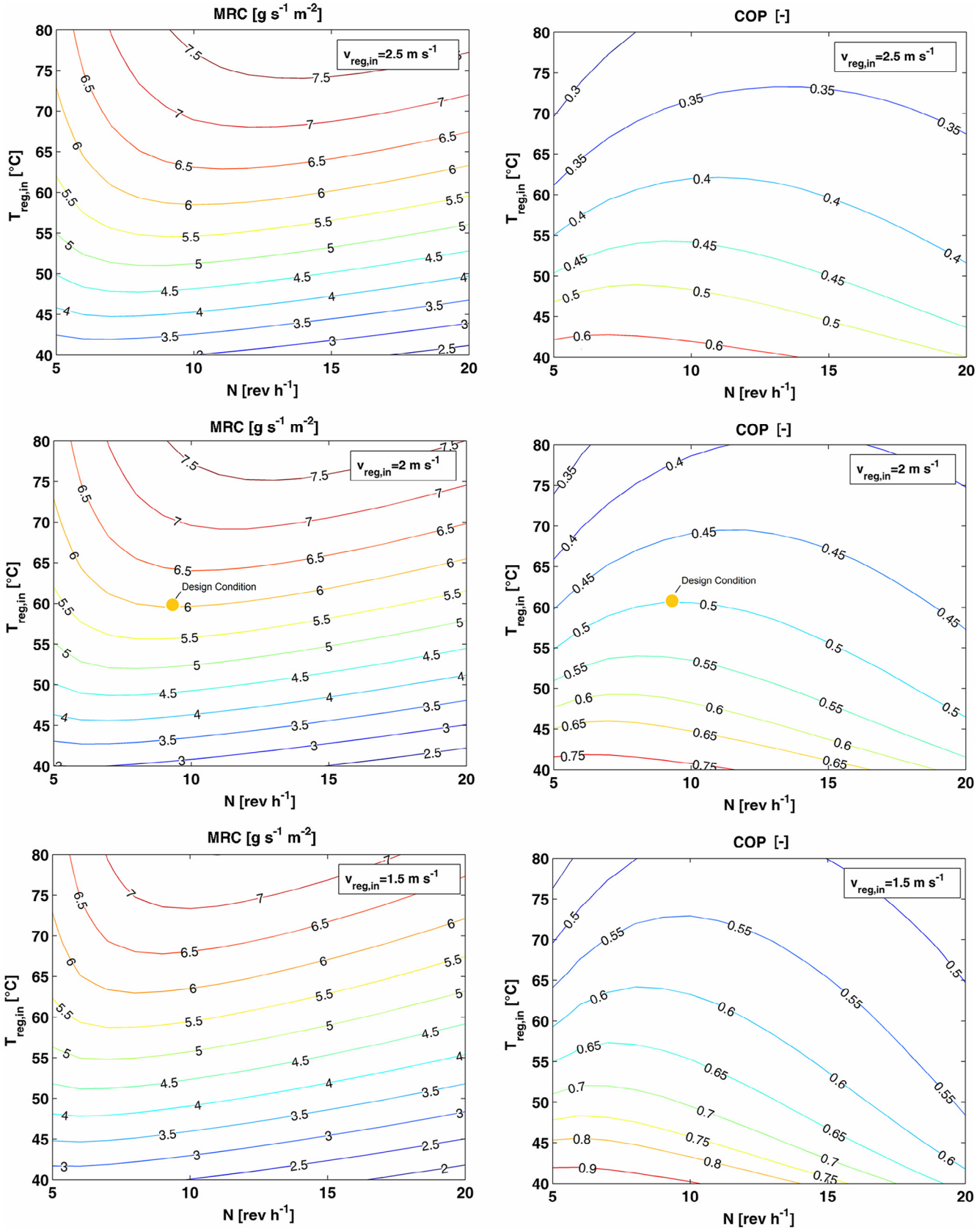

Fig. 3 – MRC and COP as a function of $T_{reg,in}$, $v_{reg,in}$ and N ($T_{pro,in}$ = 18 °C, $X_{pro,in}$ = 9.9 g kg^{-1}, $v_{pro,in}$ = 2 m s^{-1}, T_e = 32 °C, X_e = 15 g kg^{-1}).

It is highlighted that in this configuration inlet process air conditions, namely $T_{pro,in}$, $X_{pro,in}$ and $v_{pro,in}$, are constant: as a consequence, according to Eq. (7), the moisture removal capacity MRC is directly related to the supply humidity ratio X_S (or $X_{pro,out}$).

As shown in Fig. 3, maximizing MRC or COP leads to contrasting design strategies (Chung et al., 2009; De Antonellis et al., 2010). In fact, in the investigated conditions, the higher the regeneration temperature and the face velocity, the higher the dehumidification capacity and the lower the COP. Anyway, it should be pointed out that increasing $v_{reg,in}$ more than 2 m s^{-1} does not lead to a relevant improvement in MRC. In fact, in that condition that desiccant wheel matrix, at the end of the regeneration period, is already close to equilibrium with the regeneration air stream. Instead, an increase in $v_{reg,in}$ leads to an increase in q_{reg} and, therefore, in a decrease in COP. Finally, optimal revolution speed is in a relatively narrow range and it rises up with regeneration air temperature and velocity, according to previous research works (Intini et al., 2014). Quite obviously, a desiccant wheel designed to have high COP will be larger than a device designed to reach high MRC and viceversa. It is also highlighted that at constant regeneration temperature, the impact of rotation speed on MRC and COP is the same.

In this work the system design conditions are set in the following way:

- $T_{reg,in}$ = 60 °C (maximum regeneration air temperature).
- $v_{reg,in}$ = 2 m s^{-1} (maximum regeneration air face velocity, balanced volumetric air flows).
- N = 9 (optimal revolution speed).

This configuration is a good compromise between the two design approaches described above. In these conditions, the maximum moisture removal capacity is MRC_{max} = 6.046 g s^{-1} m^{-2} and the corresponding COP is equal to 0.504, as marked with orange dots in Fig. 3. The corresponding humidity ratio of the supplied air stream is X_s = 4.8 g kg^{-1}.

4.2. *Description of different control strategies*

The operating parameters that can be modified in order to balance the latent load at different boundary conditions are: the regeneration air temperature, the regeneration air velocity and the wheel revolution speed. In order to avoid an excessive complication of the system, the process air flow has been assumed constant, as in most conventional applications.

In these works, five different control strategies are proposed, as summarized in the following:

- Control A: modulation of $T_{reg,in}$ (constant $v_{reg,in}$ and N).
- Control B: modulation of $T_{reg,in}$ and N (constant $v_{reg,in}$).
- Control C: modulation of $v_{reg,in}$ (constant $T_{reg,in}$ and N).
- Control D: modulation of $v_{reg,in}$ and N (constant $T_{reg,in}$).
- Control E: modulation of $T_{reg,in}$, $v_{reg,in}$ and N.

At given latent load and boundary conditions, in cases A and C, the controlled parameter ($T_{reg,in}$ or $v_{reg,in}$) is reduced until the required MRC is reached. In case B, D and E, the two or three controlled parameters are varied and, among the possible combinations providing the required MRC, the one that maximizes the COP is chosen. Approach E represents the ideal control acting on the three aforementioned parameters.

4.3. *Part load control*

In this section, the reduction of MRC at constant outdoor and indoor air conditions is investigated. In Figs. 4 and 5 the required regeneration air temperature, air velocity and the revolution speed are shown for each control approach (orange circle and the corresponding letter). Detailed data are also reported in tables of Appendix A. The MRC is equal to 75% and 50% of MRC_{max} (6.046 g s^{-1} m^{-2} in design conditions) and the corresponding supply air humidity ratio is respectively equal to X_s = 6.1 g kg^{-1} and X_s = 7.3 g kg^{-1}. Com-

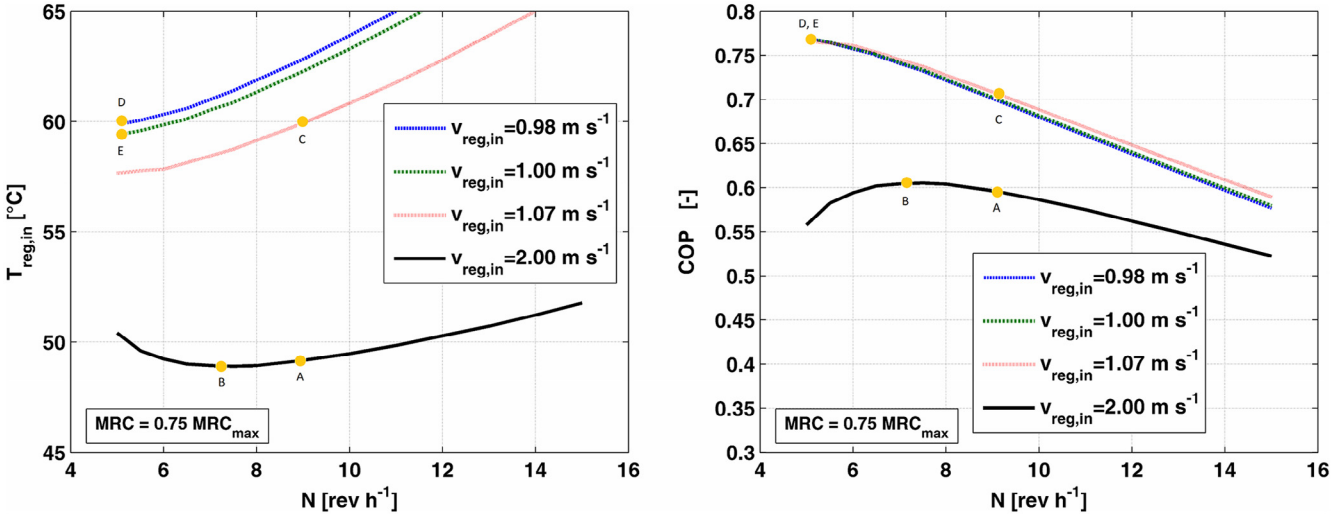

Fig. 4 – Operating conditions at part load for the five different control strategies (MRC = 4.53 g s^{-1} m^{-2}, $T_{pro,in}$ = 18 °C, $X_{pro,in}$ = 9.9 g kg^{-1}, $v_{pro,in}$ = 2 m s^{-1}, T_e = 32 °C, X_e = 15 g kg^{-1}).

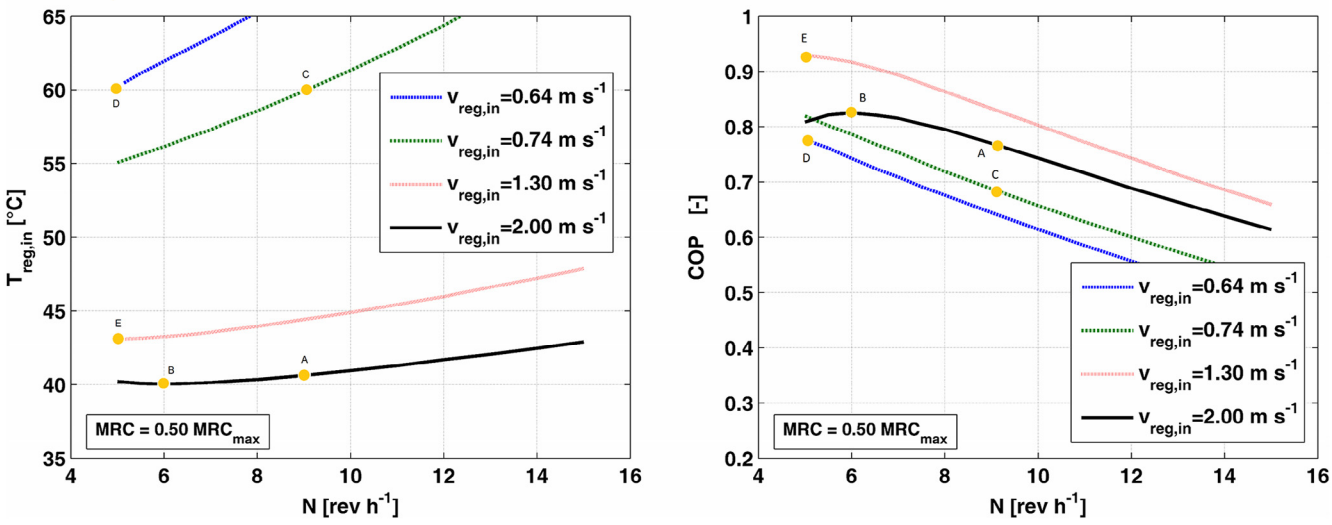

Fig. 5 – Operating conditions at part load for the five different control strategies (MRC = 3.02 g s^{-1} m^{-2}, $T_{pro,in}$ = 18 °C, $X_{pro,in}$ = 9.9 g kg^{-1}, $v_{pro,in}$ = 2 m s^{-1}, T_e = 32 °C, X_e = 15 g kg^{-1}).

paring the COP of each proposed control strategy, it is possible to state that:

- Control B does not provide a significant improvement compared to control A. In fact, due to the limited variation of the regeneration temperature (less than 20 °C at 50% of MRC_{max}) the optimal revolution speed keeps close to the one set in design conditions, as reported also in literature (Angrisani et al., 2013; De Antonellis et al., 2010; Tu et al., 2013). In addition the curve at $v_{reg,in}$ = 2 m s^{-1} is almost flat around the optimal value.
- Control D performs better than control C: the revolution speed is affected by the regeneration air flow rate and, therefore, if it is kept at the optimal condition (control D) the COP is higher.
- Control C is better than control A if MRC/MRC_{max} = 75% and it is worse if MRC/MRC_{max} = 50%. The same consideration can be done by comparing control B with control D. Generally, it is shown that it is better to reduce the MRC in the following way: first, by reducing the regeneration air flow at constant regeneration temperature and, then, by reducing the regeneration temperature at constant air flow.
- According to the previous consideration, operating parameters of control E almost coincide with ones of control D at 75% of MRC_{max}. Instead, the best regeneration air flow rate and temperature respectively increases and decreases at 50% of MRC_{max}.

The aforementioned considerations can be explained by considering the contour of MRC and q_{reg} reported in Fig. 6. A reduction in MRC can be obtained either by reducing $T_{reg,in}$ and $v_{reg,in}$, because the corresponding value of q_{reg} is proportional to the term $v_{reg,in}$ ($T_{reg,in} - T_e$). As discussed in section 4.1, at design conditions the desiccant wheel matrix at the end of the regeneration period is close to equilibrium with the regeneration air stream: a decrease in $v_{reg,in}$ leads to a slight reduction in MRC. Therefore, it is convenient to initially reduce MRC by controlling the air flow rate, which leads to a relevant reduction of q_{reg} and an increase in COP. This approach is not still valid at low values of MRC. In fact, in this case the required dehumidification is obtained by slightly heating the outdoor air: in the investigated ambient and outdoor conditions, if $T_{reg,in} = T_e$, q_{reg} is equal to zero and MRC is even still positive. This effect is clearly shown in Fig. 6, where control strategies A and C are put in evidence at MRC/MRC_{max} equal to 75% and 50% (orange dots).

4.4. *Off-design control*

In this section the reduction of outdoor air humidity ratio and temperature, at constant moisture removal capacity ($MRC = MRC_{max}$) and drying room ambient conditions is inves-

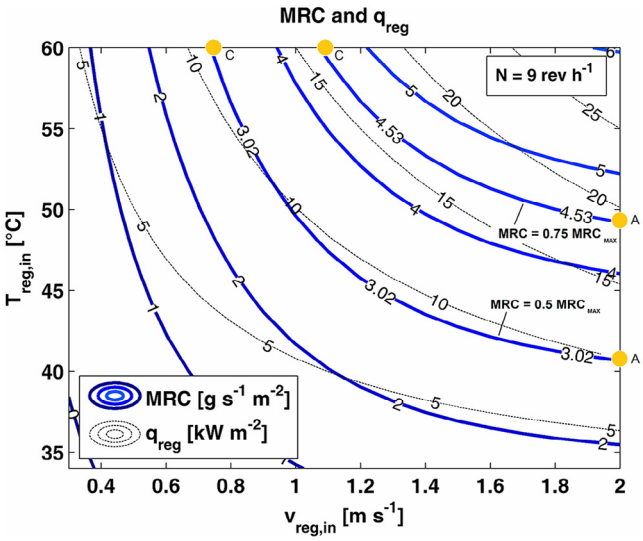

Fig. 6 – MRC and q_{reg} as a function of $T_{reg,in}$ and $v_{reg,in}$ ($T_{pro,in}$ = 18 °C, $X_{pro,in}$ = 9.9 g kg^{-1}, $v_{pro,in}$ = 2 m s^{-1}, T_e = 32 °C, X_e = 15 g kg^{-1}, N = 9 rev h^{-1}).

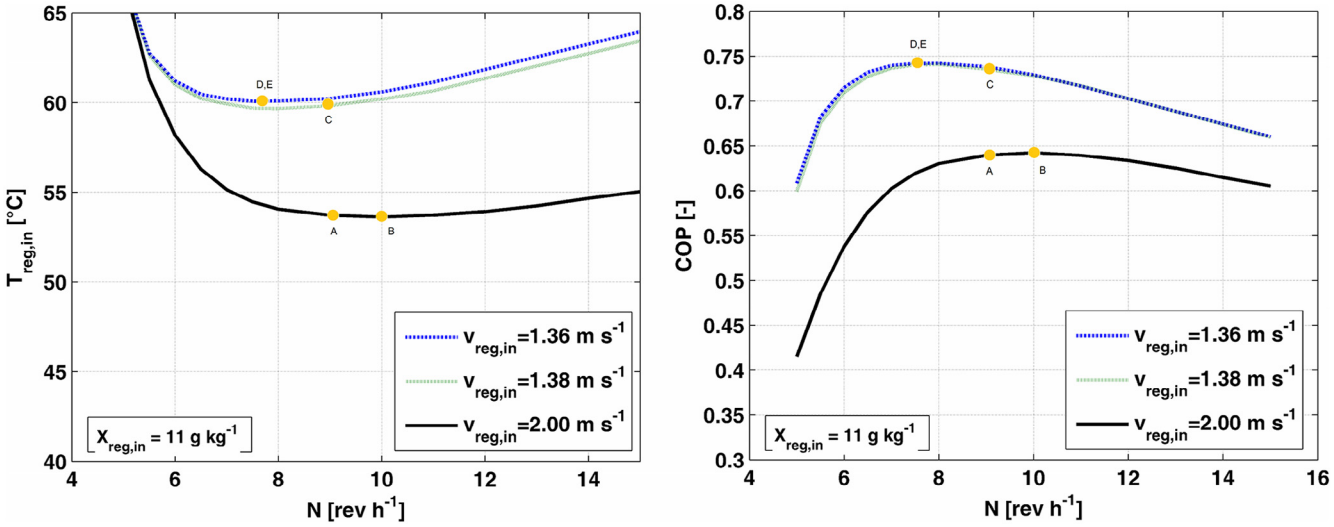

Fig. 7 – Operating conditions in off design conditions for the five different control strategies (MRC = 6.04 g s^{-1} m^{-2}, $T_{pro,in}$ = 18 °C, $X_{pro,in}$ = 9.9 g kg^{-1}, $v_{pro,in}$ = 2 m s^{-1}, T_e = 32 °C, X_e = 11 g kg^{-1}).

tigated. In Figs. 7 and 8, for each control approach, the required regeneration air temperature, air velocity and revolution speed are shown at X_e = 11 g kg^{-1} and X_e = 7 g kg^{-1}. Detailed data are listed in tables of Appendix B. Comparing the performance of each proposed control strategy, marked with a circle and the corresponding letter, it is highlighted that:

- The lower X_e (and $X_{reg,in}$), the higher the mass transfer driving force during the regeneration period and, therefore, the higher the desiccant wheel dehumidification capacity. As a consequence, $v_{reg,in}$ and $T_{reg,in}$ should be properly controlled (reduced), in order to keep MRC constant.
- The same considerations discussed in section 4.3 can be adopted in this case: if there is a slight decrease in X_e, the system is efficiently controlled by reducing $v_{reg,in}$. Instead, if X_e drops, a control of regeneration temperature at constant air flow should be preferred.
- The control of N, in addition to $T_{reg,in}$ or $v_{reg,in}$, leads to a slightly higher COP. Compared to the part load analysis, in this case, air temperature and velocity reduction are limited and, therefore, the advantage related to the control of the revolution speed is less important.
- Such considerations are confirmed in Figs. 7 and 8: control E coincides with control D (close to C) at X_e = 11 g kg^{-1} and with control B (close to A) at X_e = 7 g kg^{-1}.

Regarding the different outdoor air temperature, no significant variations occur. In fact, in this case, an independent decrease in $T_{reg,in}$ or $v_{reg,in}$ would lead to a decrease in MRC. Therefore in controls A, B, C and D, $T_{reg,in}$, $v_{reg,in}$ and N do not

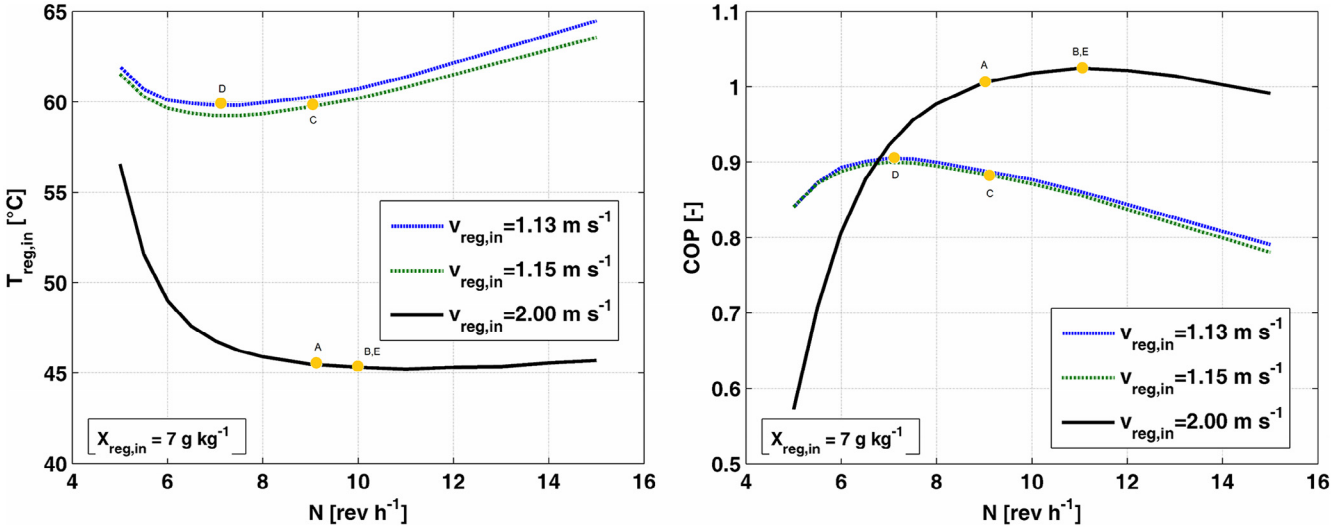

Fig. 8 – Operating conditions in off design conditions for the five different control strategies (MRC = 6.04 g s^{-1} m^{-2}, $T_{pro,in}$ = 18 °C, $X_{pro,in}$ = 9.9 g kg^{-1}, $v_{pro,in}$ = 2 m s^{-1}, T_e = 32 °C, X_e = 7 g kg^{-1}).

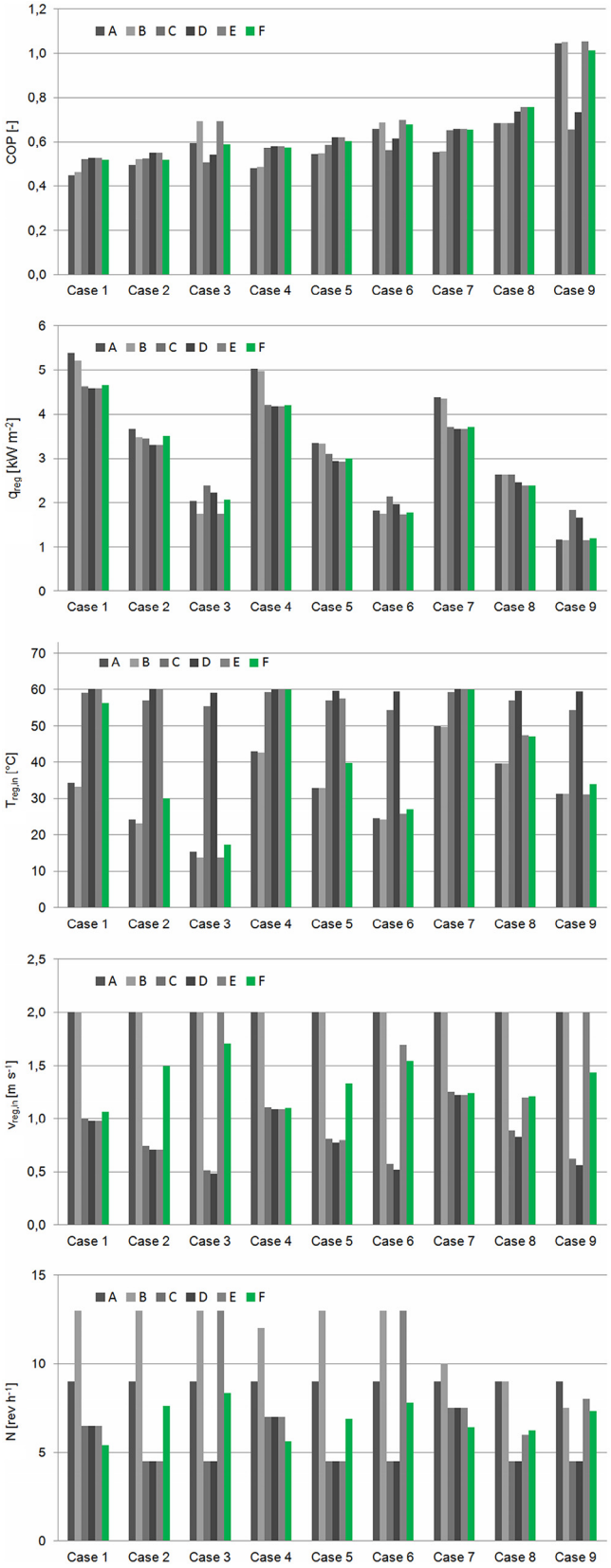

Fig. 9 – Comparison between different control strategies in cases 1–9 (Table 3).

Table 3 – Boundary conditions of the analyzed cases ($T_{pro,in}$ = 18 °C, $X_{pro,in}$ = 9.9 g kg^{-1}, $v_{pro,in}$ = 2 m s^{-1}).

Case	T_e [°C]	X_e [g kg^{-1}]	MRC/MRC$_{max}$ [%]
1	5	3	100
2	5	3	75
3	5	3	50
4	15	6	100
5	15	6	75
6	15	6	50
7	25	9	100
8	25	9	75
9	25	9	50

vary: according to Eq. (8), a reduction in T_e simply means a reduction in COP. Instead, in control E, $T_{reg,in}$ and $v_{reg,in}$ can be modified at the same time: in this case it is found that maximizing COP at constant MRC implies to raise up $T_{reg,in}$ and to reduce $v_{reg,in}$. However, since the analysis is kept with a maximum $T_{reg,in}$ equal to 60 °C, operating conditions are kept constant also in this case.

5. Analysis of a simplified control strategy

In this section a simplified control strategy is proposed and its performance is compared to controls A–E, in different outdoor air and latent load conditions. According to the considerations previously reported in sections 4.3 and 4.4, the proposed control strategy, denoted with letter F, works in the following way:

- First MRC is controlled by reducing $v_{reg,in}$ down to $v_{reg,in,min}$ = 1 m s^{-1}, with $T_{reg,in}$ = 60 °C.
- Then $T_{reg,in}$ is decreased and at the same time $v_{reg,in}$ is increased. It is assumed a linear dependence between the two parameters in the following way: $v_{reg,in} = 2 - T_{reg,in}/60$.
- The revolution speed is controlled and assumed dependent only on the regeneration air velocity in the following way: $N = -2.28\ v_{reg,in}^2 + 10.86\ v_{reg,in} - 3.56$, which has been calculated interpolating the optimal revolution speed as a function of the regeneration air velocity, at constant outdoor design conditions and at $T_{reg,in}$ = 60 °C (precisely, N_{opt} = 5, 6.5, 7.5, 8.5 and 9 rev h^{-1} respectively at $v_{reg,in}$ = 1, 1.25, 1.5, 1.75 and 2 m s^{-1}).

It is highlighted that the aim of this analysis is not to perfectly determine the best values of $v_{reg,in,min}$ and the assumed dependences between controlled parameters, but to evaluate the performance of this approach in comparison to the conventional control strategies and, in particular, to the best one denoted with letter E.

The comparison is evaluated in 9 different cases, with simultaneous variation of outdoor air temperature, humidity ratio and latent load, as summarized in Table 3.

In Fig. 9, the resulting COP and q_{reg} and the values of the parameters $T_{reg,in}$, $v_{reg,in}$ and N of each control approach are shown for the 9 cases reported in Table 3. It is highlighted that the

proposed control F is always close to the ideal control E. More precisely, q_{reg} of scenario F is higher than the one of control E by at maximum 5.7% in 8 cases (15.0% in case n° 3). Instead q_{reg} of control A, which is the typical approach adopted in real applications, is from 10.6% to 20.7% higher than the one of control E in 7 cases.

Finally, in cases 1–3, 5, and 6, the outside humidity ratio is lower than the one of the supply air stream (X_s equal to 4.8 g kg^{-1}, 6.1 g kg^{-1} and 7.3 g kg^{-1}, respectively, when MRC/MRC$_{max}$ is equal to 100%, 75% and 50%). It is highlighted that in these conditions, the latent load could also be removed through passive systems, such as enthalpy wheels or by supplying outdoor air to the drying room.

6. Conclusions

In this work, optimal control of a desiccant wheel for drying processes at part load and off design conditions is investigated. The analysis is performed through a phenomenological desiccant wheel model, which is validated with experimental data collected in typical working conditions of the investigated drying room. Five control strategies are proposed, highlighting that each one leads to significantly different heat consumption. The best approach to minimize heat consumption in conditions different from design ones, is first to reduce the regeneration face velocity and, then, to reduce the regeneration air temperature, increasing at the same time the air velocity. Finally, a simplified control approach based on the aforementioned considerations is proposed. It is shown that the simplified control can effectively reduce thermal power consumption compared to conventional control strategies, such as the ones based on the sole modulation of regeneration air temperature and flow rate. In most cases, the proposed control strategy requires around 5% more heat for regeneration than the ideal one (control E). On an average basis, in the investigated cases the COP of the simplified control approach is 7.3% and 12.1% higher than, respectively, the control based on the sole modulation of regeneration air temperature (control A) and flow rate (control C).

Appendix A

Table A1 – Resulting working conditions of different control strategies (data of Fig. 4) (MRC = 4.53 g s^{-1} m^{-2}, $T_{pro,in}$ = 18 °C, $X_{pro,in}$ = 9.9 g kg^{-1}, $v_{pro,in}$ = 2 m s^{-1}, T_e = 32 °C, X_e = 15 g kg^{-1}).

	$v_{reg,in}$ [m s^{-1}]	$T_{reg,in}$ [°C]	N [rev h^{-1}]	COP [–]
Control A	2.00	49.2	9.0	0.60
Control B	2.00	48.9	7.5	0.61
Control C	1.07	60.0	9.0	0.71
Control D	0.98	60.0	5.0	0.77
Control E	1.00	59.4	5.0	0.77

Table A2 – Resulting working conditions of different control strategies (data of Fig. 5) (MRC = 3.02 g s^{-1} m^{-2}, $T_{pro,in}$ = 18 °C, $X_{pro,in}$ = 9.9 g kg^{-1}, $v_{pro,in}$ = 2 m s^{-1}, T_e = 32 °C, X_e = 15 g kg^{-1}).

	$v_{reg,in}$ [m s^{-1}]	$T_{reg,in}$ [°C]	N [rev h^{-1}]	COP [–]
Control A	2.00	40.6	9.0	0.77
Control B	2.00	40.0	6.0	0.83
Control C	0.74	60.0	9.0	0.69
Control D	0.64	60.0	5.0	0.78
Control E	1.30	43.1	5.0	0.93

Appendix B

Table B1 – Resulting working conditions of different control strategies (data of Fig. 7) (MRC = 6.04 g s^{-1} m^{-2}, $T_{pro,in}$ = 18 °C, $X_{pro,in}$ = 9.9 g kg^{-1}, $v_{pro,in}$ = 2 m s^{-1}, T_e = 32 °C, X_e = 11 g kg^{-1}).

	$v_{reg,in}$ [m s^{-1}]	$T_{reg,in}$ [°C]	N [rev h^{-1}]	COP [–]
Control A	2.00	53.7	9.0	0.64
Control B	2.00	53.6	10.0	0.64
Control C	1.38	60.0	9.0	0.73
Control D	1.36	60.0	7.5	0.74
Control E	1.36	60.0	7.5	0.74

Table B2 – Resulting working conditions of different control strategies (data of Fig. 8) (MRC = 6.04 g s^{-1} m^{-2}, $T_{pro,in}$ = 18 °C, $X_{pro,in}$ = 9.9 g kg^{-1}, $v_{pro,in}$ = 2 m s^{-1}, T_e = 32 °C, X_e = 7 g kg^{-1}).

	$v_{reg,in}$ [m s^{-1}]	$T_{reg,in}$ [°C]	N [rev h^{-1}]	COP [–]
Control A	2.00	45.5	9.0	1.01
Control B	2.00	45.3	10.0	1.02
Control C	1.15	60.0	9.0	0.89
Control D	1.13	60.0	7.0	0.90
Control E	2.00	45.3	10.0	1.02

REFERENCES

Angrisani, G., Minichiello, F., Roselli, C., Sasso, M., 2011. Experimental investigation to optimise a desiccant HVAC system coupled to a small size cogenerator. Appl. Therm. Eng. 31 (4), 506–512.

Angrisani, G., Roselli, C., Sasso, M., 2013. Effect of rotational speed on the performances of a desiccant wheel. Appl. Energy 104, 268–275.

Bourdoukan, P., Wurtz, E., Joubert, P., 2010. Comparison between the conventional and recirculation modes in desiccant cooling cycles and deriving critical efficiencies of components. Energy 35 (2), 1057–1067.

Chung, J.D., Lee, D.Y., Yoon, S.M., 2009. Optimization of desiccant wheel speed and area ratio of regeneration to dehumidification as a function of regeneration temperature. Sol. Energy 83 (5), 625–635.

Dai, Y.J., Wang, R.Z., Xu, Y.X., 2002. Study of a solar powered solid adsorption – desiccant cooling system used for grain storage. Renew. Energy 25 (3), 417–430.

Daou, K., Wang, R.Z., Xia, Z.Z., 2006. Desiccant cooling air conditioning: a review. Renew. Sustain. Energy Rev. 10 (2), 55–77.

De Antonellis, S., Joppolo, C.M., Molinaroli, L., 2010. Simulation, performance analysis and optmization of desiccant wheels. Energy Build. 42, 1386–1393.

De Antonellis, S., Joppolo, C.M., Molinaroli, L., Pasini, A., 2012. Simulation and energy efficiency analysis of desiccant wheel systems for drying processes. Energy 37, 336–345.

De Antonellis, S., Intini, M., Joppolo, C.M., 2015a. Desiccant wheels effectiveness parameters: correlations based on experimental data. Energy Build. 103 (15), 296–306.

De Antonellis, S., Intini, M., Joppolo, C.M., Molinaroli, L., Romano, F., 2015b. Desiccant wheels for air humidification: an experimental and numerical analysis. Energy Convers. Manag. 106, 355–364.

DIN EN ISO 5167-2 Standards, 2003. Measurement of Fluid Flow by Means of Pressure Differential Devices Inserted in Circular Cross-Section Conduits Running Full – Part 2: Orifice Plates. ISO 5167-2:2003.

Elgendy, E., Mostafa, A., Fatouh, M., 2015. Performance enhancement of a desiccant evaporative cooling system using direct/indirect evaporative cooler. Int. J. Refrigeration 51, 77–87.

Ge, T.S., Dai, Y.J., Wang, R.Z., 2014. Review on solar powered rotary desiccant wheel cooling system. Renew. Sustain. Energy Rev. 39, 476–497.

Goldsworthy, M.J., White, S.D., 2011. Optimization of a desiccant cooling system design with indirect evaporative cooler. Int. J. Refrigeration 34, 148–158.

Hands, S., Sethuvenkatraman, S., Peristy, M., Rowe, D., White, S., 2016. Performance analysis & energy benefits of a desiccant based solar assisted trigeneration system in a building. Renew. Energy 85, 865–879.

Intini, M., De Antonellis, S., Joppolo, C.M., 2014. The effect of inlet velocity and unbalanced flows on optimal working conditons of Si-Gel desiccant wheels. Energy Procedia 48, 858–864. Intini, M., De Antonellis, S., Joppolo, C.M., Casalegno, A., 2015. A trigeneration system based on polymer electrolyte fuel cell and desiccant wheel – part B: overall system design and energy performance analysis. Energy Convers. Manag. 106, 1460–1470.

ISO IEC Guide 98-3, 2008. Uncertainty of Measurement – Part 3: Guide to Expression of Uncertainty in Measurement. International Organization for Standardization, Geneva Switzerland. ISO IEC Guide 98-3.

Jeong, J., Yamaguchi, S., Saito, K., Kawai, S., 2011. Performance analysis of desiccant dehumidification systems driven by low-grade heat source. Int. J. Refrigeration 34, 928–945.

Lee, D.Y., Kim, D.S., 2014. Analytical modeling of a desiccant wheel. Int. J. Refrigeration 42, 97–111.

Ling, J., Kuwabara, O., Hwang, Y., Radermacher, R., 2013. Enhancement options for separate sensible and latent cooling air-conditioning systems. Int. J. Refrigeration 2013, 45–57.

Liu, W., Lian, Z., Radermacher, R., Yao, Y., 2007. Energy consumption analysis on a dedicated outdoor air system with rotary desiccant wheel. Energy 32 (9), 1749–1760.

Misha, S., Mat, S., Ruslan, M.H., Salleh, E., Sopian, K., 2015. Performance of a solar assisted solid desiccant dryer for kenaf core fiber drying under low solar radiation. Sol. Energy 112, 194–204.

Nagaya, K., Li, Y., Jin, Z., Fukumuro, M., Ando, Y., Akaishi, A., 2006. Low temperature desiccant-based food drying system with airflow and temperature control. J. Food Eng. 75, 71–77.

Panaras, G., Mathioulakis, E., Belessiotis, V., 2011. Proposal of a control strategy for desiccant air-conditioning systems. Energy 36 (9), 5666–5676.

Rambhad, K.S., Walke, P.V., Tidke, D.J., 2016. Solid desiccant dehumidification and regeneration methods – a review. Renew. Sustain. Energy Rev. 59, 73–83.

Ruivo, C.R., Costa, J.J., Figueiredo, A.R., 2007. On the behaviour of hygroscopic wheels: part II – rotor performance. Int. J. Heat Mass Transf. 50, 4823–4832.

Sultan, M., El-Sharkawy, I.I., Miyazaki, T., Saha, B.B., Koyama, S., 2015. An overview of solid desiccant dehumidification and air conditioning systems. Renew. Sustain. Energy Rev. 46, 16–29. Tu, R., Liu, X.H., Jiang, Y., 2013. Performance comparison between enthalpy recovery wheels and dehumidification wheels. Int. J. Refrigeration 36, 2308–2322.

Vitte, T., Brau, J., Chatagnon, N., Woloszyn, M., 2008. Proposal for a new hybrid control strategy of a solar desiccant evaporative cooling air handling unit. Energy Build. 40 (5), 896–905.

Wang, W.C., Calay, R.K., Chen, Y.K., 2011. Experimental study of an energy efficient hybrid system for surface drying. Appl. Therm. Eng. 31, 425–431.

White, S.D., Goldsworthy, M.J., Reece, R., Spillmann, T., Gorur, A., Lee, D.Y., 2011. Characterization of desiccant wheels with alternative materials at low regeneration temperatures. Int. J. Refrigeration 34, 1786–1791.

Zouaoui, A., Zili-Ghedira, L., Ben Nasrallah, S., 2016. Open solid desiccant cooling air systems: a review and comparative study. Renew. Sustain. Energy Rev. 54, 889–917.